Available online at www.sciencedirect.com
ScienceDirect
Nuclear Instruments and Methods in Physics Research A 580 (2007) 1513–1521
NUCLEAR INSTRUMENTS & METHODS IN PHYSICS RESEARCH Section A
www.elsevier.com/locate/nima

High precision axial coordinate readout for an axial 3-D PET detector module using a wave length shifter strip matrix

A. Braem[a], E. Chesi[a], C. Joram[a,*], J. Séguinot[a], P. Weilhammer[a], R. De Leo[b], E. Nappi[b], W. Lustermann[c], D. Schinzel[c], I. Johnson[d], D. Renker[d], S. Albrecht[e]

[a]*CERN, PH Department, CH-1211 Geneva, Switzerland*
[b]*INFN, Sezione di Bari, I-70122 Bari, Italy*
[c]*ETH Zürich, CH-8092 Zürich, Switzerland*
[d]*Paul Scherrer Institut, CH-5232 Villigen, Switzerland*
[e]*University Hospital Geneva, CH-1211 Geneva, Switzerland*

Received 11 May 2007; received in revised form 25 June 2007; accepted 28 June 2007
Available online 23 July 2007

Abstract

We describe a novel method to extract the axial coordinate from a matrix of long axially oriented crystals, which is based on wavelength shifting (WLS) plastic strips. The method allows building compact 3-D axial gamma detector modules for PET scanners with excellent 3-D spatial, timing and energy resolution while keeping the number of readout channels reasonably low. A voxel resolution of about 10 mm^3 is expected. We assess the performance of the method in two independent ways, using classical PMTs and G-APDs to read out the LYSO (LSO) scintillation crystals and the WLS strips. We observe yields in excess of 35 photoelectrons from the strips for a 511 keV gamma and reconstruct the axial coordinate with a precision of about 2.5 mm (FWHM).

PACS: 87.58.Fg; 85.60.Ha; 85.40.−e

Keywords: PET; Santillator; HPD; G-APD

1. Introduction

Advances in Positron Emission Tomography (PET) are driven to a significant extent by progress in instrumentation, i.e. by the performance of scintillation crystals, photodetectors and readout electronics. We describe a novel method to extract the axial coordinate from a matrix of long axially oriented crystals, which is based on wavelength shifting (WLS) plastic strips. The method allows building compact high performance 3-D axial gamma detector modules for PET scanners.

The paper is organised as follows: in Section 2 we motivate the development by medical requirements arising from functional PET imaging, particularly in the fields of brain research and oncology. Section 3 describes the current limitations of PET instrumentation and points out how our proposed concept can contribute to overcoming them. The principle and potential of the WLS based readout is discussed in Section 4, while Section 5 describes the experimental demonstration of the method. In Section 6 we summarize and give an outlook on our next steps.

2. Medical requirements for optimal brain PET scanning

Functional imaging using PET has become one of the most powerful methods in medical imaging to study and quantify metabolic processes in the human (and animal) body. In particular PET plays a crucial role in quantification of the brain function. Advances in brain PET imaging, where emphasis is put on accurate observation of small structures, rely on improving the spatial resolution and the sensitivity of present day PET scanners, if possible

*Corresponding author.
E-mail address: Christian.Joram@cern.ch (C. Joram).

0168-9002/$ - see front matter © 2007 Elsevier B.V. All rights reserved.
doi:10.1016/j.nima.2007.06.107

combined with reduced radiation exposure of the patient. Another important issue will be the possibility to combine a PET scanner with other precise morphological imaging devices like X-ray CT and MRI in co-registration mode. Some specific medical considerations illustrating the importance of such improvements are discussed below for the case of brain scanning. Clearly, such improvements would also benefit other medical PET applications,
e.g. positron emission mammography (PEM) or in-beam PET scanning in Hadron Therapy Installations.

Brain PET is used to cover a broad clinical field of applications ranging from oncology to neurology, psychiatry and vascular diseases. In all cases a significant improvement of image quality and sensitivity of the PET scanner will contribute strongly to improve diagnostics and treatment of the patient. To illustrate this a few examples will be discussed.

In neuro-oncology 18F-FDG (Fluoro-2-deoxy-D-glucose), which is an analogue of glucose and as such incorporated into active cells using the glucose transport mechanism on the basal membrane, can be used to distinguish viable tumour tissue from scar tissue after radiation therapy. The elapsed time after radiotherapy plays an important role as it creates a state of inflammation of up to 4 weeks after its end leading to an increase of background activity and a decrease of the tumour to background ratio. To use the full potential of PET imaging in this particular therapy an improvement of performance of PET scanners is crucial.

Recently a new tracer, FET (Fluoro-ethyl-tyosine), which is a cell proliferation marker, has attracted much attention. FET-PET is more and more used in the work-up of glioma in adults. FET-PET with high spatial resolution can spot additional lesions of very little volume that sometimes have not been diagnosed by routine 4 MRI. In addition, it can visualize a highly active hypermetabolic region within the suspected brain tumour indicating the most aggressive component of a tumoral lesion. Multimodality imaging could substantially contribute to precise localisation of lesions and thus metabolic and anatomical information can guide the neurosurgical stereotactic biopsy for histopathological analysis. These results help to correctly classify the primary brain tumour and evaluate prognostic factors to choose the adequate treatment option.

Examples of other applications, which would benefit from significant improvements in PET performance, are brain PET with FDG in epilepsy diagnostic and treatment and F-DOPA-PET for imaging movement disorders.

In conclusion one can state that there is a strong medical case for improvements of sensitivity, spatia l resolution and image quality in PET scanners. Medical analysis and interpretation of symptoms in a wide field of brain deceases, as shown in the few examples above, will greatly be helped by improving the performance of PET scanners as proposed in this paper.

3. Overcoming limitations of present clinical PET scanners

PET scanners of the present generation use radial geometry with rather finely segmented scintillation crystals and Anger logic readout. The main limitations in acquiring images with the best possible spatial resolution and image contrast, while having reasonably high detector efficiency, such that the patient is only exposed to an as small as possible radiation dose, are summarised in the following: parallax error due to limited knowledge of the depth of interaction in the scintillation crystal of the 511 keV photon (in the radial direction); relatively low efficiency of photon conversion due to the anti-correlation between accurate knowledge of depth of interaction and radial thickness ($=$ length) of scintillation crystals; image smearing due to the physics of the photon interaction, since Compton scattering is always dominating over the photo absorption process even for the highest Z scintillation crystals and limited capability to identify and reject events with Compton interactions in the scintillation material.

A reference for a new generation of PET scanners is the High Resolution Research Tomograph (HRRT) [1–3] developed by CPS Innovation (Knoxville, USA) and under test since several years. In this PET scanner the Phoswich arrangement [1] of crystals reduces at a given efficiency image smearing due to DOI uncertainty. Effic iency for the detection of photon pairs is given to be 6.9%, which includes a sizeable fraction of unidentified Compton interactions. Energy resolution is 17% at 511 keV and timing resolution is 2–4 ns. The volumetric voxel resolution is given as $20\,mm^3$, corresponding to a trans-axial resolution of 2.6 mm in average and an axial resolution of about 3 mm. All quantities referenced here are FWHM.

The ultimate limitations in accuracy caused by the physics process of positron emission and annihilation is in most cases small compared to the performance in spatial resolution of presently available PET scanners. For the commonly used isotope ^{18}F the effect of the finite range of the positron before annihilation contributes a projected spatial uncertainty of only 0.13 mm, but a considerably bigger FW(0.1)M value of $\sim$ 1 mm due to tails in the distribution can contribute to image blurring. Rather important effects on the deterioration of image resolution can be expected for isotopes with higher end point positron energies like ^{124}I, ^{15}O or ^{94}mTc.

The other irreducible smearing in spatial resolution of PET scanners comes from the non-colinearity of the photon pairs ($\sim \pm 0.25^\circ$) due to the finite momentum distribution of the e^+e^- system at the moment of annihilation. The strength of this effect scales obviously with the diameter of the PET ring and is less important for small animal PET Scanners.

Our previously proposed concept of a true 3-D PET scanner with axial geometry of the scintillation crystals [4] has a number of very attractive features; however, the determination of the axial (z) coordinate was based on the light intensity ratio measured at the two ends of the crystals

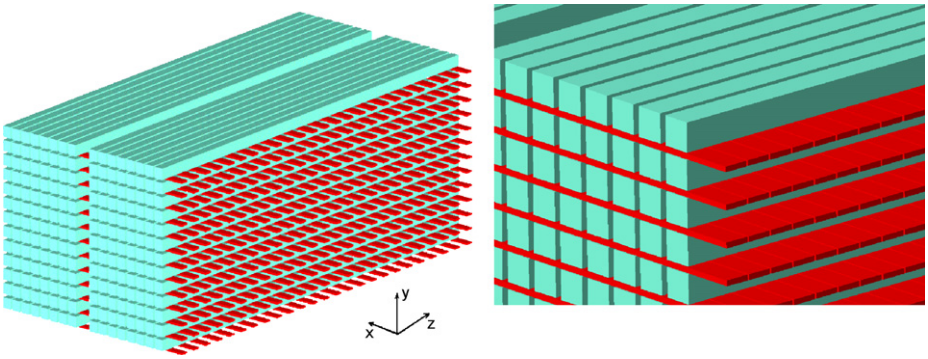

Fig. 1. Left: principle of readout of a scintillator matrix with wavelength shifting strips. For reasons of clarity only every second WLS strip is shown. Right: zoomed view with all WLS strips shown.

with Hybrid Photon Detectors [4]. In this paper we propose a novel approach which will allow to obtain equally good spatial resolution in x, y and z coordinates by introducing an array of plastic WLS strips oriented orthogonal to the axis of the crystals.

The novel concept features all the improvements and advantages, which were part of the original proposal [4]: the most important of these were true 3-D reconstruction with uniformity of spatial resolution over the complete field of view, the concept has inherently no parallax error, high efficiency independent of spatial resolution (no limitations to the radial thickness of the scintillation stack) and capability to identify Compton interaction with nearly 100% efficiency, allowing to increase sensitivity by a factor ~1.6. The introduction of WLS arrays further improves the axial geometry configuration. It offers the possibility to choose, independently of other device parameters, the spatial resolution needed for a given application by an appropriate choice of crystal and wavelength shifter strip dimensions (as shown later a volumetric voxel resolution of $\sim 10\,\mathrm{mm}^3$ for brain PET is realistic), it provides equal spatial resolution in all three dimensions and finally allows the possibility of simultaneous co-registration of, e.g. PET and MRI by using very fast new photodetectors, Geiger Mode APD arrays (G-APD, also called SiPM), for the readout of scintillation crystal bars and WLS strips.

4. Readout of the z-coordinate of an axial PET scanner with WLS strips

In the new concept discussed in this paper the z-coordinate is obtained by introducing an orthogonal layer of stacks of thin WLS strips between the layers of the scintillation crystal matrix (Fig. 1). The scintillation crystal stack consists of ~ 15 cm long LYSO crystals with a cross-section of 3.2 mm × 3.2 mm, axially oriented and separated by 0.8 mm. Each array of 16×13 crystals is optically coupled at one end to appropriate fast photon detector arrays, with an aluminium coating applied on the opposite side reflecting the light to the readout side. The thin WLS strips are arranged as z-hodoscopes placed in the 0.8 mm wide air gaps between crystal rows.

The role of the crystal matrix is now limited to the reconstruction of the x-and y-coordinates and to the measurement of the deposited energy. The crystals are optimised for long absorption length, i.e. for light yield and ultimately energy resolution.

The WLS strips are excited by the scintillation light (e.g. LSO: $\lambda \sim 420$ nm) which is not trapped in the crystal by total internal reflection (see Fig. 2). A major part of the scintillation light escaping from the crystal bars is absorbed by the WLS strip and re-emitted as fluorescence light at about 490 nm (Y-11 WLS). A fraction of the fluorescence light is trapped in the strip by total internal reflection and propagates to the two end faces of the strip. One end face is mirror-coated reflecting the light to the opposite end, where it is detected by compact fast photosensors.

Reading out scintillators with wavelength shifter bars, strips or fibres is a widely used method in calorimetry of high energy physics experiments where the light from a large scintillator volume needs to be concentrated on a relatively small photodetector. The readout of crystals for medical applications via plastic scintillators and strips is already documented in literature [5]. However, to the best of our knowledge, the specific geometry proposed here has not been implemented before.

The photoelectric yield of the WLS strip can be roughly estimated as

$$N/E_\gamma(\mathrm{MeV}) = Y_\mathrm{L} \cdot \frac{\mathrm{d}\Omega}{4\pi} \cdot \frac{1}{4} \cdot \varepsilon_\mathrm{fluor} \cdot \varepsilon_\mathrm{trans} \cdot \varepsilon_\mathrm{det}. \quad (1)$$

We use the following parameters: light yield of LYSO scintillator $Y_\mathrm{L} = 32.000\,\mathrm{MeV}^{-1}$, solid angle of nontrapped scintillation photons $\mathrm{d}\Omega/4\pi = 0.19$ (Monte Carlo), measured fluorescence efficiency of the WLS material $\varepsilon_\mathrm{fluor} = 0.8$, measured trapping and transport efficiency (due to optical absorption) $\varepsilon_\mathrm{trans} = 0.5$, photon detection efficiency of the sensor (in this calculation a PM tube) $\varepsilon_\mathrm{det} = 0.15$ (at 490 nm). This results in $N/E_\gamma = 46$ detected photoelectrons (pe) for a 511 keV gamma which would guarantee 100% detection efficiency and allow to determine the z-coordinate, along the crystal axis, both in digital and analogue form.

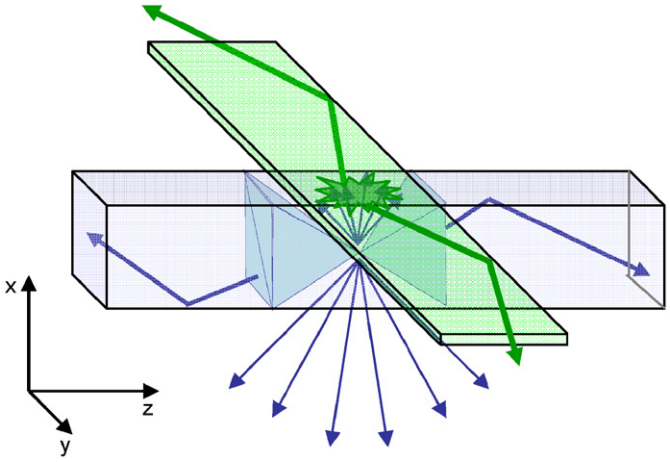

Fig. 2. Details of scintillation and fluorescence light trapping. Only one crystal and one WLS bar are shown.

If only the signal from one WLS strip with width d closest to the photon interaction in the LYSO crystal is taken one obtains a digital spatial resolution ($\sigma = d/\mathrm{SQRT}(12)$) which can be tuned by varying the width of the WLS strips. For hits where the conversion of a 511 keV photon in the LYSO crystal is seen by more than one WLS strip, the z-coordinate can be determined by a centre of gravity algorithm requiring that the readout electronics provides analogue information. For such events one might expect that the z-resolution is even better than digital resolution.

Geiger mode Avalanche PhotoDetectors (G-APDs) are very good candidates for the readout of the WLS strips, e.g. the Hamamatsu MPPC 33-050C Multi-Pixel Photon Counter. G-APDs are particularly interesting for this application because of their compactness, speed, relatively good linearity and energy resolution. In addition, they can be operated in very high magnetic fields which allow combing PET with CT and MRI. The effective photon detection efficiency at 490 nm is expected to be of the order 30%.[1]

For the readout of the crystal matrix both a single HPD mounted at one end or G-APDs reading the light on one or on both ends of the matrix can be considered. In the case of HPD readout suppressing the readout on one side allows for a more compact arrangement of the crystal matrices in a full scanner, essentially free of cracks. Using G-APDs will also provide very good timing resolution thus helping to reduce random coincidence background.

With an attenuation length for annihilation photons of more than 30 cm in polystyrene WLS strips and an attenuation length of about 1 cm in LYSO, only $\sim 1\%$ of 511 keV photons will interact in the WLS strips. This small fraction of undesired events will be eliminated by energy cuts on the signals of the scintillation crystals.

The proposed PET architecture is very attractive for other applications like PEM or very high resolution small animal platforms. In the case of a small animal axial PET scintillation crystal stacks could be built with single crystals of 1–2 mm side dimensions and only 4–6 cm length. A very compact small animal PET scanner with 3-D sub-millimeter resolution in the image space and very high sensitivity could be realised.

Use of long scintillation crystals may seem prohibitive for TOF-PET, an approach which relies on sub-ns timing to improve noise and NEC rate characteristics and brings also other advantages [6]. The precise knowledge of the axial position of the photon's interaction eliminates the fluctuation from the unknown propagation time along the crystal and restores the full resolution. As will be shown below, readout of a long crystal with G-APDs leads to a very competitive TOF resolution.

5. Experimental demonstration of the WLS based z-readout

Two different and independent approaches were followed to assess the potential of the WLS based z-readout. In the following we sketch the principles and the test set-ups and summarize the main results. We concentrate on three topics: (1) the photoelectric yield of the WLS strips, (2) the achievable spatial resolution along the crystal axis and (3) the timing resolution. A more detailed description of the experimental techniques and the results will be given in a forthcoming article.

5.1. Principle and experimental set-up

The photon detector in a PET scanner is required to precisely localize gamma rays in the energy range between about 100–511 keV. The low energy range is of particular interest for the 3-D-axial camera, as it is used to unambiguously discriminate Compton interactions in the crystal matrix. We demonstrate the principle and performance of the WLS based z-readout with two different and independent methods, which are schematically shown in Fig. 3.

1. *Pulsed low energy electron source*: In order to vary the energy deposition in the scintillator crystal and its position in an easily controllab le way, we designed a set-up which is based on a pulsed source of low energy electrons which impinge on the crystal. The electrons are produced by illuminating a semitransparent CsI photocathode with short light pulses ($\sim$10 ns) from a H2 flash lamp. The negative potential of the photocathode U_{cath} ($10 \leqslant U_{\mathrm{cath}} \leqslant 27.5$ kV) defines the kinetic energy of the electrons when they hit the crystal surface. The total energy deposition is controlled through the number N_e of electrons in the pulse. Two LYSO:Ce crystals ($3.2 \times 3.2 \times 100\,\mathrm{mm}^3$) were mounted side by side, with one of their end faces optically coupled through a Sapphire window to a single photomultiplier tube.[2] The other end

[1] Data Sheet Humamatsu MPPC 33-050C.

[2] Photonis XP3102. Photonis, Brive La Gaillarde, France.

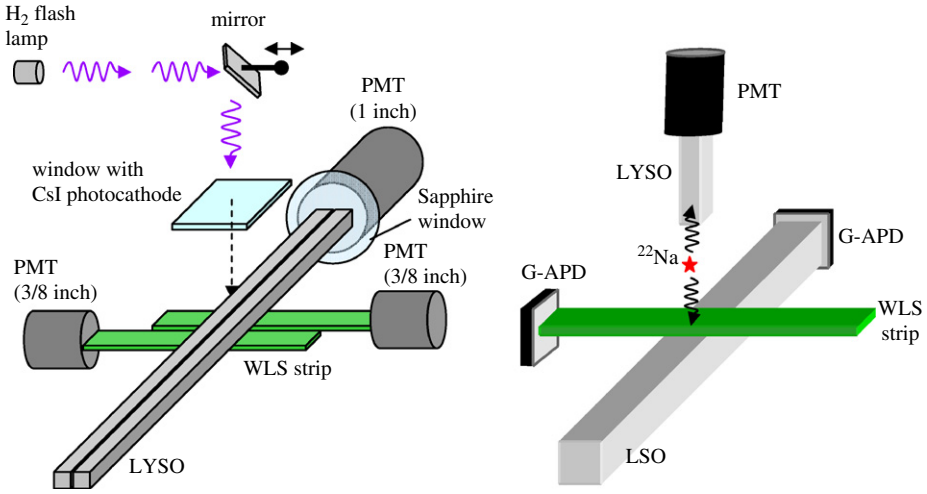

Fig. 3. Schematic representation (not to scale) of the two measurement principles. Left: set-up with low energy electron source. Right: set-up with ^{22}Na source.

faces are mirror-coated with a vacuum evaporated Al film. Two 60 mm long WLS strips[3] ($3 \times 1.1\,mm^2$) were 10 mounted orthogonal to and underneath the two crystals with a small air gap of about 0.1 mm. An aluminium foil under the strips reflects the small fraction of non-absorbed light back onto the strip. The strip end which is not readout was also coated with a reflective aluminium film. The set-up allows continuously varying the deposited energy and displacing the beam spot in a controlled way in order to measure the z-resolution of the WLS based readout. The beam spot at the level of the crystals has Gaussian shape with FWHM of 1.8 mm, both in the x and y coordinate. The available intensity of the collimated H_2 flash lamp allowed energy depositions up to about 425 keV per pulse. The measurements needed to be performed in vacuum.

2. *Radioactive ^{22}Na source*: In the second set-up a smaller LSO crystal ($3 \times 3 \times 50\,mm^3$) and an orthogonal WLS strip (same type and dimensions as above) were exposed to annihilation photons from a ^{22}Na source. Both the crystal and the WLS strip were readout at one end by a G-APD of $3 \times 3\,mm^2$ size.[4] A small LYSO crystal ($2 \times 2 \times 12\,mm^3$) readout by a PMT served to tag the second annihilation photon. The non-read end of the LSO crystal was closed with white Teflon tape and three of the long sides were covered with reflecting foil (V2000 from 3 M). The upper side of the strip was covered with a reflecting foil and the non-read end with Teflon tape.

In both set-ups conventional optical grease was used to improve the light transmission between scintillators (WLS strips) and photodetectors.

[3]ELJEN EJ-280, high dye concentration, SCIONIX, Bunnik, The Netherlands.

[4]Type MPPC 33-050C Hamamatsu Photonics, Hamamatsu City, Japan.

5.2. Results with the pulsed low energy electron source

The scintillation crystals are excited by short bunches of low energy electrons. In first approximation, the total energy deposited in the crystal per bunch is $E_{dep} = N_e$ $E_e = N_e \cdot e \cdot U_{cath}$. For relatively small numbers N_e of electrons per bunch (e.g. <30), the fluctuation $\sigma(N_e) = \sqrt{N_e}$ dominates over the photon statistics and the intrinsic resolution of the scintillator. The number of electrons in the bunch and hence the deposited energy can therefore be determined from $N_e = (Q/\,\sigma(Q))^2$ with Q and $\sigma(Q)$ being the charge amplitude and its fluctuation, respectively, measured with the PMT connected to the LYSO crystal. The charge amplitude Q is obtained by integrating the PMT signal with a charge sensitive ADC (LeCroy 1182, gate length 150 ns). Absolute calibration of the PMTs' gains was performed by determining the response of the PMTs to single pe generated by a pulsed LED. This allows converting the measured charge to the number of detected pe.

The analysis is complicated by two low energy effects: (1) a fraction (~45%) of the electrons is backscattered from the LYSO crystal without depositing their full energy. (2) The light yield of LYSO scales with the deposited energy in a non-linear way, described by the Relative Light Output function RLO.[5] A straightforward Monte Carlo model, based on measured backscattering and light yield data [7–9] is used to describe the two effects and to derive from the measured charge and its fluctuation, Q and $\sigma(Q)$, the actually converted energy. We estimate the relative precision of the MC corrected energy value to be $\pm 10\%$.

Fig. 4 shows the measured charge distribution from the LYSO crystal for a total converted energy of 366 keV ($N_e = 25$, $E_e = 27.5$ keV, $E_{dep} = 443$ keV). After conversion to pe using the calibration of the PMT, the variation

[5]Above E_e 20 keV, $RLO \sim 0.76$ For $E_e > 100$ keV, RLO is essentially equal to 1.

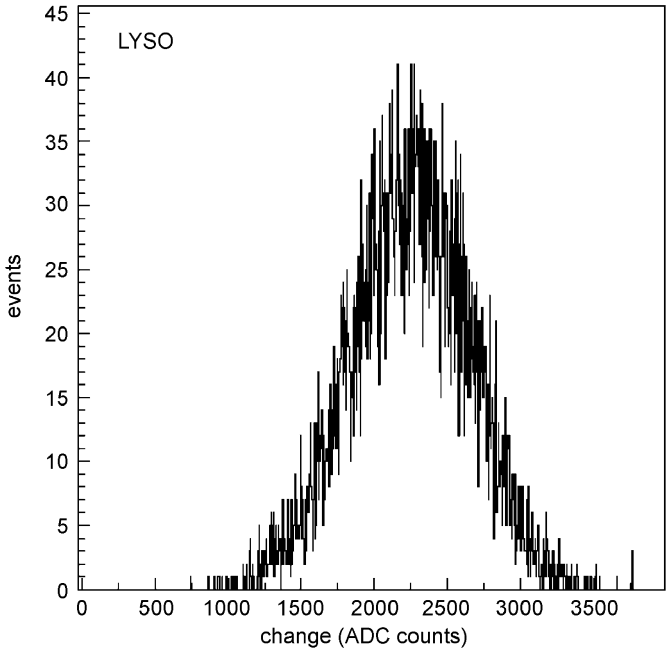

Fig. 4. Integrated charge signal, extracted from the LYSO crystal (in ADC counts; 1 count = 50 fC) following excitation with $N_e \sim 25$ electrons of 27.5 keV energy.

of the photoelectric yield with the converted energy is shown in Fig. 5. Extrapolation to 511 keV yields a photoelectric yield of 1160 pe. It should be noted that such a photoelectric yield, if produced by a single 511 keV photon, and not by a group of low energy electrons, would lead to an energy resolution of about 10–11% (FWHM).[6] Fig. 6 shows the charge distributions for the two WLS strips (with the source in a fixed position between the two WLS strips) and Fig. 7 the variation of the sum of the measured charges from the two strips with the converted energy. The extrapolated value of the photoelectric yield at 511 keV was found to be 42, a value which guarantees full detection efficiency.

The z-coordinate, i.e. the coordinate transverse to the strips along the crystals, can be reconstructed using the yield ratio of the two WLS strips:

$$z_{\mathrm{rec}} = a + b \cdot \frac{Q_1 - Q_2}{Q_1 + Q_2}. \quad (2)$$

The parameters a (= offset) and b (= slope) need to be adjusted once. Fig. 8 shows the reconstructed z-coordinate versus the position of the beam spot derived from the mirror position (see Fig. 3, left). In the region of the WLS strips, which are indicated in the figure, the coordinate varies linearly with the mirror position. Outside the WLS strips, signals are seen only in the closer WLS strip resulting in a constant value for the reconstructed coordinate. The width of the z_{rec} distribution as function of the converted energy is shown in Fig. 9. It shows the

[6] $\Delta E/E = 2.35(F/N_e + R_i^2)^{1/2}$ with $F \sim 1.2$ (excess noise factor of PMT) and $R_i \sim 3\%$ (intrinsic resolution of LYSO).

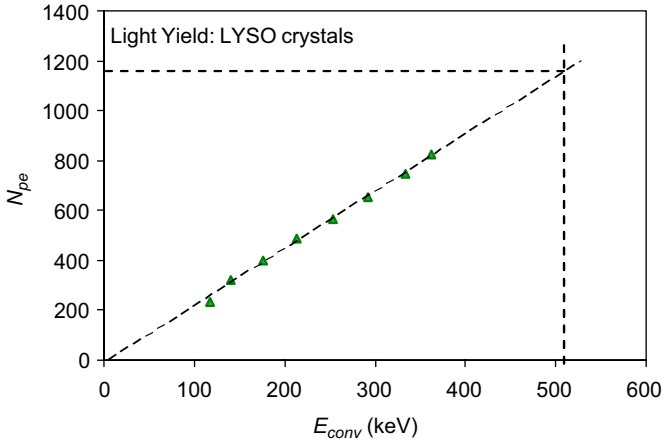

Fig. 5. LYSO crystal: dependence of the photoelectric yield, derived from the charge signal, on the converted energy.

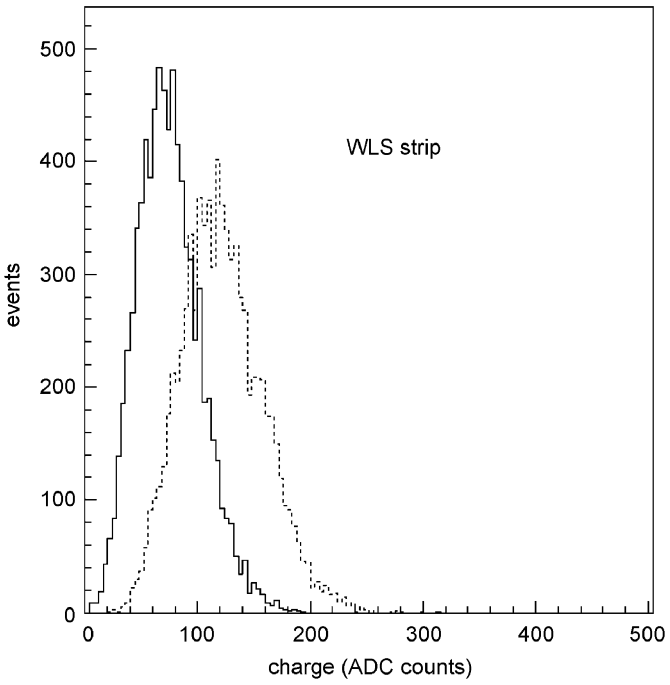

Fig. 6. Charge distributions, extracted from the two WLS strips for a fixed source position (in ADC counts; 1 count = 50 fC).

expected $1/\sqrt{E_{\mathrm{conv}}}$ dependence. Extrapolation to 511 keV leads to a z-resolution of 1.1 mm.

The analysis was complemented by a Monte-Carlo study in order to disentangle the contribution of the finite size of the beam spot (1.8 mm FWHM) and to clarify a possible impact of the depth of the light emission in the crystal. The MC predicted for the above experimental configuration, where the scintillation light is produced just under the top surface of the crystals, a resolution of $\sigma_z = 0.95$ mm (compared to the measured 1.1 mm). For point like light emission, randomly distributed over the full crystal thickness, a resolution of 0.6 mm is predicted.

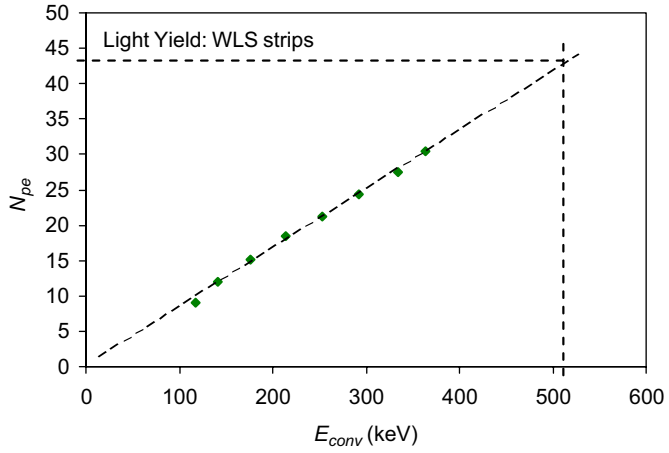

Fig. 7. WLS strips: dependence of the photoelectric yield, derived from the charge signal, on the converted energy. The sum of the two WLS strips is shown.

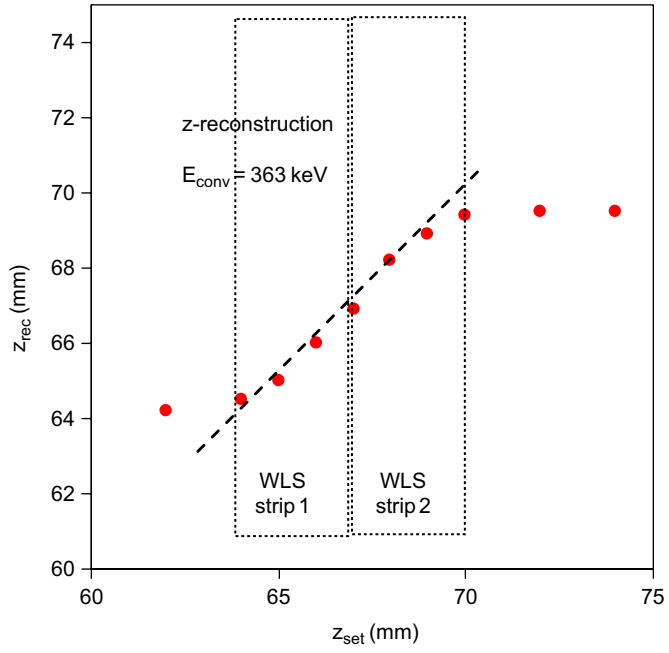

Fig. 8. Reconstructed z-coordinate (for a converted energy of 363 keV) versus the z-coordinate of the electron beam. The position of the two 3 mm wide WLS strips is indicated. If the beam spot is placed besides the strips, such that the light is detected only by one strip, the reconstruction algorithm produces by construction (see Eq. (2)) a constant value.

5.3. Results obtained with the ^{22}Na source

The signals of both G-APDs (cf. Fig. 3) were amp lified by a factor of ~20 using the MAR-8[7] amplifier and fed into a timing filter amplifier (Ortec 454) with gain 1 and 50 ns shaping time. The signals from the two crystals readout by a G-APD and a photomultiplier, respectively, were sent to constant fraction discriminators. Their outputs formed a

[7]Mini-Circuits, New York (US), www.minicircuits.com.

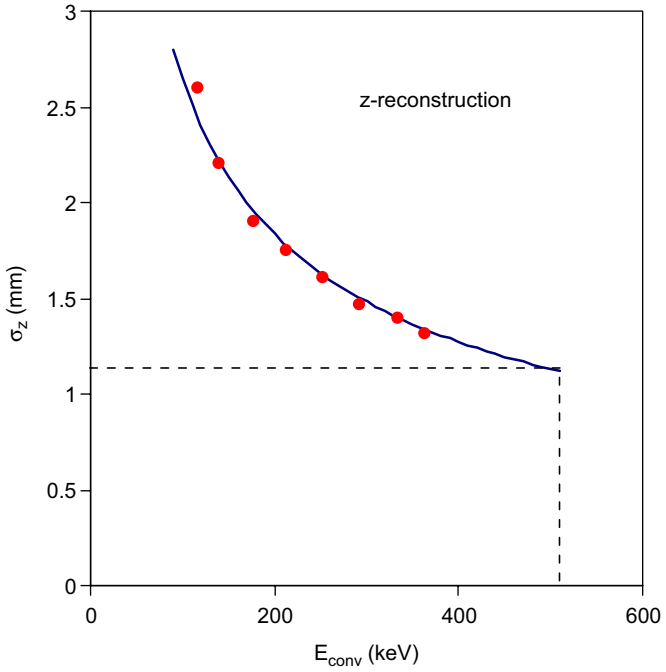

Fig. 9. The reconstruction precision is plotted versus the converted energy. Extrapolation to 511 keV indicates a precision of $\sigma_z = 1.1$ mm.

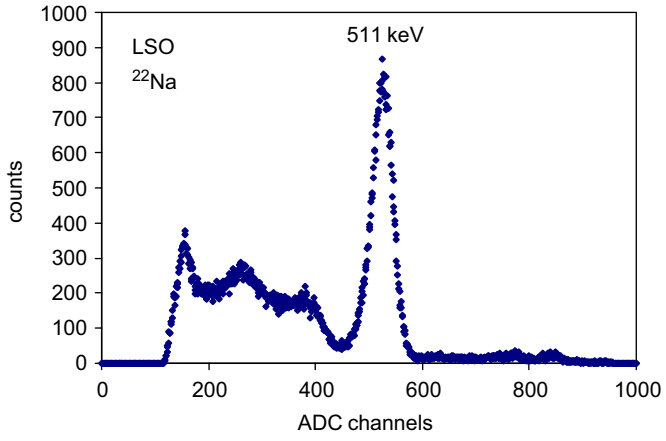

Fig. 10. Integrated charge spectrum of the LSO/G-APD detector.

coincidence which opened the gate of a charge sensitive ADC. The spectrum obtained with the LSO/G-APD detector is shown in Fig. 10. For the 511 keV X-rays an energy resolution of 11.5% FWHM was obtained, in good agreement with the value estimated from photoelectric yield measurements which were performed on the e-source set-up, discussed before.

The signal from the WLS/G-APD detector was recorded by the ADC using the same gate derived from the coincidence. The threshold of the LSO/G-APD discriminator was set between the Compton edge and the 511 keV line, thus selecting only photoelectric events. The resulting charge spectrum is shown in Fig. 11.

The excellent resolution of G-APDs for one, two, etc. pe allows a simple and precise calibration of the spectrum.

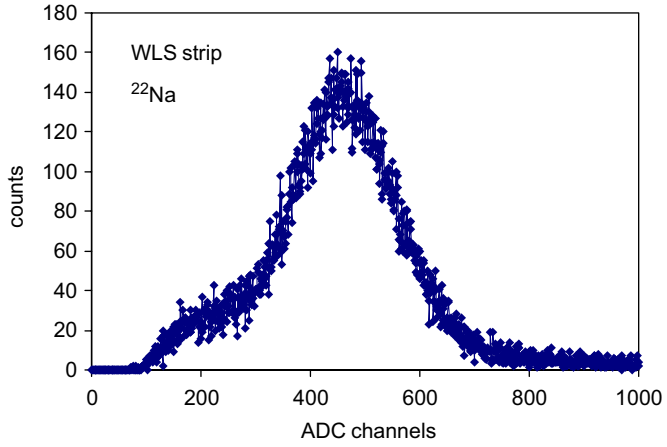

Fig. 11. Pulse height spectrum of the WLS/G-APD detector when only photoelectric events are selected.

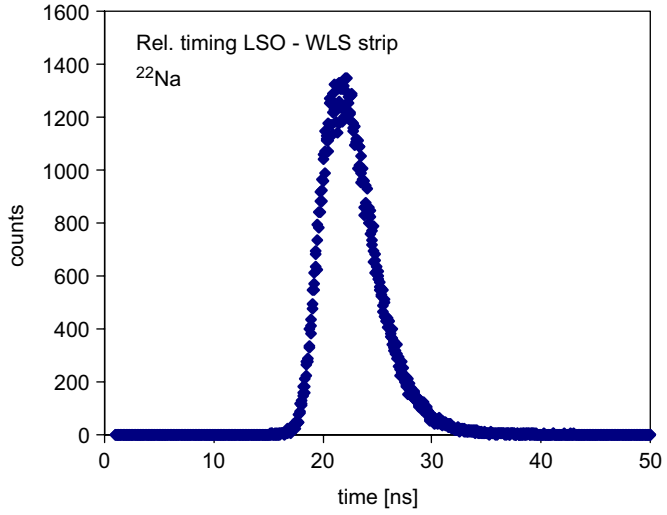

Fig. 12. Relative timing between the LSO crystal and the WLS strip, both readout with G-APD. Only photoelectric events were selected. The combined resolution is 5.5 ns (FWHM).

A value of 8.8 ADC channels/pe was found. Using this calibration the photoelectric peak of Fig. 11 corresponds to 43.5 pe.

In a G-APD photons from an avalanche in a hit microcell leaking to neighbouring cells leads to cross-talk, which increases with gain. The cross-talk increases the number of hit cells and therefore the apparent charge. We estimate the $3 \times 3\,mm^2$ Hamamatsu device to have a cross-talk of 10–20% for the gain values used in this measurement. Hence the true photoelectric yield of the WLS strip is therefore 35–39.

The relative timing between the LSO crystal and the WLS strip was measured with a TDC and constant fraction discriminators. The threshold of the constant fraction discriminator of the LSO/G-APD which defined the start signal was set to select only photoelectric events. The constant fraction discriminator connected to the WLS strip was set to ~2pe and was used as stop signal. From the TDC spectrum shown in Fig. 12 the resolution was determined to be 5.5 ns (FWHM). The contribution of the LSO crystal was extracted from a TDC spectrum using the small tagging LYSO/PMT detector as stop signal and was found to be 700 ps (FWHM) indicating that the WLS strip completely dominates the relative timing precision.

5.4. Discussion and comparison of the results

We demonstrated with two independent methods the readout of WLS strips which detect the scintillation light of LYSO/LSO crystals. In both cases a comfortably high photoelectric yield was achieved which even exceeds the rough performance estimates based on simple considerations. The yield figures allow efficient detection and precise spatial reconstruction.

The performance achieved with the G-APD readout of the LSO crystal in terms of energy and time resolution is comparable to or better than recent published data [10].

The photoelectric yield obtained by both methods cannot be compared directly since the photon detection efficiency of the G-APD at 490 nm is about two times higher than the one of the bialkali photocathode of the PMT. In addition, the single WLS strip equipped with a G-APD does not have full geometric acceptance for the detection of the scintillation light. The two effects compensate each other to a certain extent for this particular measurement.

6. Summary and next steps

We propose a detector concept for PET scanners where long axially oriented scintillation crystals are readout on one end. The axial z-coordinate is derived from a hodoscope made of thin WLS strips slotted in between the crystals. Our measurements, performed with two different and independent set-ups, using classical PMT and novel G-APD for the readout, proved the feasibility of this geometrical configuration and demonstrated that an excellent z-resolution of better than $\sigma_z = 1.1$ mm can be achieved at $E = 511$ keV.Given the transverse size of the scintillator crystals, a voxel resolution of about $10\,mm^3$ (FWHM) appears fully realistic.

We intend to fabricate a small demonstrator module, based on a matrix of, e.g. 4×4 or 5×5 long LYSO crystal bars. An appropriate arrangement of WLS strips, e.g. 4×16 or 4×32 strips, slotted in between the crystals will be used for the axial coordinate reconstruction. Such a module allows characterizing energy and z resolution of the matrix and studying integration related effects like cross-talk between different strip layers.

A small demonstrator module will also allow studying various readout options. The crystals can be read with an existing HPD [11] developed previously and tested for the Axial HPD-PET project [4]. The WLS strips can be read with G-APDs. Alternatively, both crystals and strips can be read with G-APDs. The conception and fabrication of

an appropriate multichannel readout ASIC for arrays of G-APDs is a logical step in the sequence.

The availability of two small demonstrator modules would allow performing studies in PET configuration and assessing the potential of the proposed geometrical configuration under realistic conditions.

Acknowledgement

We would like to thank our technical staff, C. David, A. Folley, M. van Stenis, (all CERN), L. Dell'Olio and G. De Carne (INFN Bari) for their excellent work in the preparation of the mechanical and optical components used in the tests. Two of us (W.L. and D.S.) are very grateful to Prof. F. Pauss for her continuous support. We are also indebted to M. Droege, Chr. Haller, Drs F. Nessi-Tedaldi and P. Lecomte for the set-up of a test bench.

References

[1] M. Schmandt, et al., Performances results of a new DOI detector block for a High Resolution PET LSO Re-search Tomograph HRRT, IEEE Trans. Nucl. Sci. (1998) 3000.

[2] K. Wienhard, et al., The ECAT HRRT: Performance and first clinical application of the new high resolution research tomograph, IEEE Trans. Nucl. Sci. NS- 49 (2002) 104.

[3] M. Schmand, K. Wienhard, M.E. Casey, et al., Performance evaluation of a new LSO High Resolution Research Tomograph—HRRT, in: J.A. Seibert (Ed.), Proceedings of the IEEE 1999 Nuclear Science Symposium and Medical Imaging Conference, Vol. 2, Seattle, WA, 1999, Paper M04-002, pp. 1067–1071.

[4] J. Séguinot, et al., Novel geometrical concept of a high performance brain *PET* scanner—principle, design and performance estimates, Il, Nuovo Cimento C 29 (04) (2006) 429.

[5] N. Belcari, et al., Measurement of photoelectron yield from scintillating fibres coupled to a YAP:Ce matrix, Nucl. Instr. and Meth. A 461 (2001) 413.

[6] W.W. Moses, Time of flight in PET revisited, IEEE Trans. Nucl. Sci NS-50 (5) (2003) 1325.

[7] W. Mengesha, et al., IEEE Trans. Nucl. Sci. NS-45 (3) (1998) 456.

[8] W.W. Moses, Current trends in scintillator detectors and materials, Nucl. Instr. and Meth. A 487 (2002) 123.

[9] E.H. Darlington, Backscattering of 10–100 keV electrons from thick targets, J. Phys. D 8 (1975) 85.

[10] E. Lorenz, et al., Some studies for a development of a small animal PET based on LYSO crystals and Geiger mode-APDs, Nucl. Instr. And Meth. A 572 (2007) 259.

[11] E. Chesi, et al., A segmented Hybrid Photon Detector with integrated auto-triggering front-end electronics for a PET scanner, Nucl. Instr. and Meth. A 564 (2006) 352.